Available online at www.sciencedirect.com
SCIENCE DIRECT
Earth and Planetary Science Letters 246 (2006) 197–206
EPSL
www.elsevier.com/locate/epsl

Low fault friction in Iran implies localized deformation for the Arabia–Eurasia collision zone

P. Vernant *, J. Chéry

Laboratoire Dynamique de la Lithosphère, CNRS–Université de Montpellier II, CC 060, place E. Bataillon, 34095 Montpellier Cedex 05, France

Received 22 August 2005; received in revised form 31 March 2006; accepted 7 April 2006
Available online 30 May 2006
Editor: Scott King

Abstract

The GPS velocity field of the present-day deformation in Iran is modeled using a 3-dimensional (3D) finite element approach. The deformation can be accommodated either by a continuum medium or by faults which are modeled using discontinuities with Coulomb-failure criteria. Depending on the fault friction, the deformation will be accommodated by the continuum medium or by the faults. Therefore, no a priori hypothesis on continuum or microplate behavior is assumed. In addition, geological fault slip rates are used to better determine the optimum model. The best model fitting both GPS and geological data shows quasi-rigid blocks within the deformation zone and low effective fault friction for the main Iranian strike slip faults. The mechanical behavior of the Iranian lithosphere seems to be partly controlled by the large strike slip faults. However, some deformation is still taken up by the continuum medium, suggesting a compromise between the microplate and continuum descriptions. Results also suggest localized shear zones in the mantle underneath the crustal faults bordering the quasi-rigid blocks. Lastly, the Arabia push relative to Eurasia explains most of the kinematics in Iran, but the complex velocity field of the surrounding South Caspian basin cannot be fitted by this model. Therefore, slab pull due to a remnant oceanic crust may occur in the Caucasus–Caspian region.

Keywords: Iran; fault slip rate; 3D modeling; GPS

1. Introduction

Two extreme descriptions have been suggested to describe active tectonic deformation [1]. The first one is based on microplate behavior, assuming the deformation is localized on faults bordering rigid blocks. This description is in good agreement with the present day velocity field of the Anatolian region (e.g., [2–7]) and of California (e.g., [8]). Several authors used a microplate model to describe Central Asia deformation (e.g., [9–11]). However, the mechanical behavior of the Central Asian lithosphere is still an ongoing debate and continuum descriptions (i.e., quasi-continuous flow) have been used for this region (e.g., [12,13]). Unfortunately, GPS coverage of this region remains too scarce [14] to definitely conclude which model is the most appropriate. Recent GPS studies in Iran [15–18] bring new data (Fig. 1) on the kinematics of intracontinental deformation. The geodetic rate of Arabia–Eurasia convergence appears to be in good agreement with geological studies [19], suggesting a constant strain rate over at least the last 10 Ma. In addition, GPS confirms the quasi-rigid behavior of the

* Corresponding author. Current address: Earth, Atmospheric and Planetary Sciences Department, Massachusetts Institute of Technology, 54-617, 77 Massachusetts avenue, Cambridge, MA 02139-4307, USA.
E-mail address: vernant@mit.edu (P. Vernant).

0012-821X/$ - see front matter © 2006 Elsevier B.V. All rights reserved.
doi:10.1016/j.epsl.2006.04.021

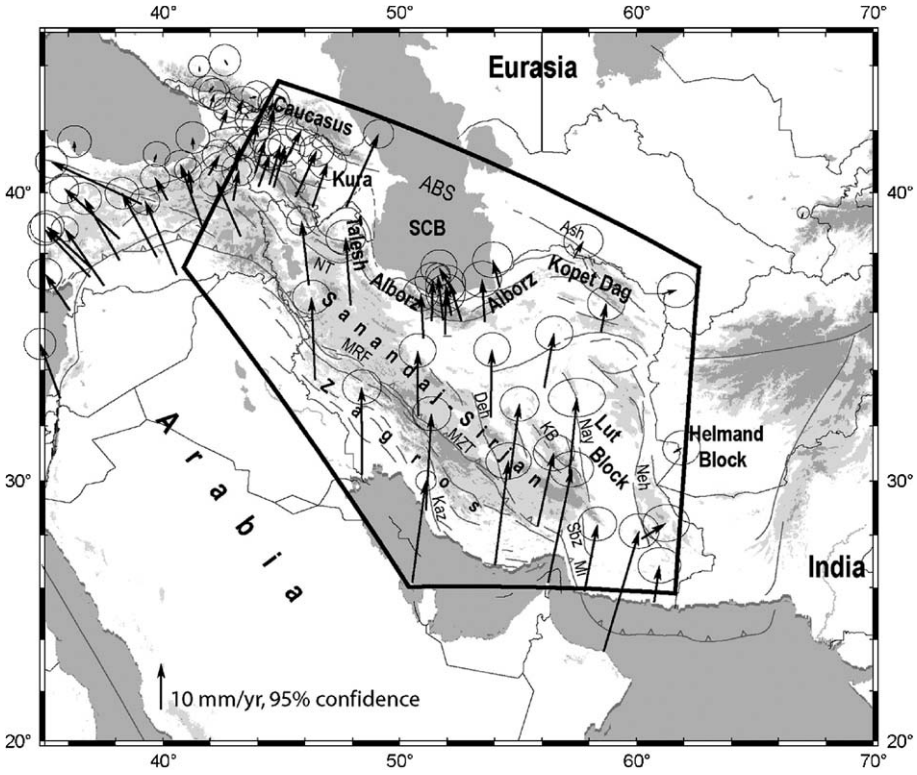

Fig. 1. Simplified tectonic map and GPS velocity field of the study area. The GPS horizontal velocities and their 95% confidence ellipses are in Eurasia-fixed reference frame (compilation of results from the studies by McClusky et al. [3]; Vernant et al. [17,18]). The heavy black-contour polygon shows the boundaries of our model. ABS: Apsheron Balkan Sills, Ash: Ashkabad fault, SCB: South Caspian Basin/Block, Deh: Dehshir fault, Kaz: Kazerun fault, KB: Kuh Banan fault, Kura: Kura Basin, Mi: Minab–Zendan–Palami fault zone, MRF: Main Recent fault, MZT: Main Zagros thrust, Nay: Nayban, NT: North Tabriz fault, Sbz: Sabzevaran fault.

Central Iranian Block (Fig. 1) which seems to be limited to the Sanandaj–Sirjan zone. If the Arabia/Eurasia collision rate seems to be steady over the last 10 Ma, the tectonic has changed inside the collision zone and most of the present-day active faults are younger than ~5 Ma [20]. However short-term (10 yrs) and long-term slip rate (10,000 yrs to 5 Ma), when available, usually agree within their uncertainties [7].

Previous numerical models of Iranian deformation have been constructed using the assumption of a continuum deformation [21,22], but without direct constraints on the velocity field in Iran. Using GPS and geological data available in Iran, we use mechanical modeling to infer the effective rheological properties involved in the last stage (~5 Ma) of the Arabia–Eurasia intracontinental collision zone.

2. Model

Mechanical modeling has been extensively used to study the link between strain, stress and the rheological properties of the lithosphere. Using cross-sections and two-dimensional approaches, several convergent zones have been studied (e.g., [23–27]) taking into account the rheological complexity of the lithosphere with plastic and viscous constitutive laws. Models in three dimensions have also been presented, but due to their numerical complexity they have been used mainly to describe simple geometrical settings (e.g., [28–30]). For deformation of a large area such as the Tibetan plateau, a rheological simplification of the lithosphere is used with a thin viscous sheet model (e.g., [12,13,31]). However, this model does not take into account the plastic (or frictional) deformation of the lithosphere in the upper crust and possibly the uppermost mantle. Therefore, the hypothesis of a strong upper crust driving the collision kinematics cannot be tested. The thin viscous sheet model has been applied to Iran by Jackson et al. [21] and Sobouti and Arkani-Hamed [22]. Both of these studies concluded that deformation of the Iranian lithosphere is determined by the shape of the rigid boundaries and the disposition of the rigid blocks within the collision zone. In this study, we used a three-dimensional finite element model (ADELI 3D [32]) to account for the rheological

properties of the Iranian lithosphere, including both pressure and temperature dependent bulk rheological laws and fault discontinuities.

2.1. Constitutive laws and numerical formulation

The constitutive laws used are pressure–temperature (P–T) dependent (Fig. 2). For both upper crust and mantle, we use an elastoplastic pressure-dependent law with a Drucker–Prager failure criterion [27,33]. The friction angle is set to 15° to be consistent with a high internal friction (μ=0.6) and a hydrostatic pore pressure for the upper crust [29]. At high P–T, a strain rate dependent "power law" rheology is approximated by a linear Maxwell model of viscoelasticity in which the fluidity γ (Pa^{-1} s^{-1}) depends on the temperature T as follows:

$$\gamma = \gamma_0 e^{-E/RT}$$

where γ_0 is a material constant, E is the activation energy and R is the gas constant. The rheological change between the upper seismogenic crust and the lower viscous crust depends on the temperature gradient of the region. We use a quartz-controlled rheology for the crust and a dunite-controlled rheology for the mantle except at low temperature for which a plastic yield stress of 600 MPa is assumed [34–36]. For example, assuming a typical strain rate of 10^{-15} s^{-1} we obtain effective crustal viscosities of 10^{23} Pa s at 350 °C and 10^{20} Pa s at 650 °C in order to model the viscosity decrease in the lower crust [37]. The effective viscosities for the mantle are 10^{22} Pa s at 600 °C and 10^{21} Pa s at 800 °C. Due to the strong thermal dependence of the viscosity and the lack of constraints on the thermal model, lateral variations of the lithosphere rheology result from variations of the assumed model temperature rather than by adjusting the constitutive law parameters.

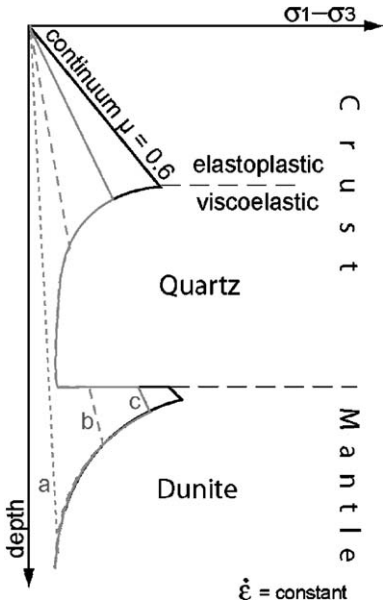

Fig. 2. Rheological properties of the lithosphere used in the model. The black curve is for the continuum medium. The grey lines represent faults, with effective fault friction increasing from (a) to (c). Note that for a very low effective fault friction, the fault can cross most of the lithosphere.

The main Iranian faults are introduced in the model using finite element mesh discontinuities, and the effective fault friction μ is modeled using Signorini and Coulomb laws [27]. Contact forces are computed between all nodes belonging to the discontinuity between the top surface to the bottom of the model (120 km). To allow localization of the deformation on faults, the fault strength must be lower than that of the continuum medium (Fig. 2). In the case of a very low effective fault friction and a low to moderate geotherm, the fault slip discontinuity can cross all the lithosphere (case a on Fig. 2). Effective fault friction can be set to different values between the crust and the mantle, allowing us to limit the fault displacement to the crust. There is a trade-off between fault friction and fault slip rate (e.g., [38]); therefore, it seems that a best fit could be obtained by using different fault frictions depending on the fault. However, for the sake of a simple interpretation we choose to keep the same fault friction for all faults in one experiment, we only vary it from one experiment to the other.

Internal, external and contact forces are used to compute the acceleration of the mesh nodes. Velocities and displacements are computed using a dynamic relaxation method [27,39]. Time stepping is chosen to be small enough to make out of balance forces negligible. Therefore, a quasi-static solution of the balance equation is obtained.

2.2. Geometry

The geometry and boundary conditions of our model are shown in Fig. 3, and the geographical boundaries are superimposed on the topographic map of Fig. 1. Our model extends from Eastern Turkey (west) to Afghanistan (east), and from the Persian Gulf and Makran (south) to the Caucasus and the Kopet Dag (north). It is approximately 1800×1800 km^2 along the X (W–E) and Y (S–N) axes. The lithosphere is modeled for a flat Earth (non-spherical geometry) and gravity forces are included. The normal crust thickness is set to 35 km (with ρ_c=2800 kg/

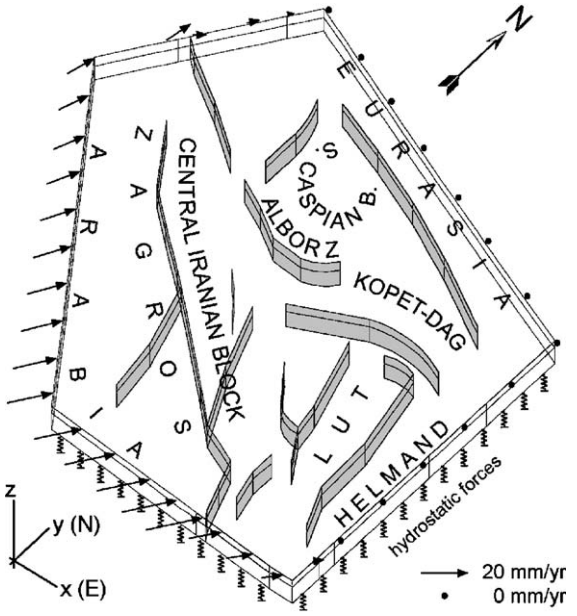

Fig. 3. Geometry of the model. The model includes the entire deformation zone between the Arabian and Eurasian plates at the longitude of Iran (see location on Fig. 1). The crust and upper mantle are simulated by two layers and the base of the mantle is subject to hydrostatic forces. Faults are represented by the grey vertical plane. The boundary conditions correspond to the rigid motion of Arabia in a Eurasia-fixed reference frame deduced from the GPS observations. The western and eastern border velocity gradients are estimated between each GPS sites on these borders.

m^3), but we included the topography averaged over areas of 40×40 km^2, and computed an isostatically compensated crustal root. Except in the Alborz region where the range might not be isostatically compensated, our crustal root fits quite well the Moho geometry computed by Dehghani and Makris [40] based on gravity data. The upper mantle (with $\rho_m=3300$ kg/m^3) extends from the Moho to the base of the model at 120 km depth. The base is submitted to hydrostatic forces in order to simulate the interaction with a fluid asthenosphere.

The main Iranian faults are modeled using vertical discontinuities (Fig. 3) extending from the surface to the base of our model. Due to mesh limitations, we can include only vertical faults. Therefore, these faults will only accommodate strike slip motions and the shortening will be taken up by the continuum medium. However, the larger Iranian faults are mainly strike–slip faults according to geological evidence, except for the Main Zagros Thrust (MZT, Fig. 1). Hence we only infer the importance of the strain localization for the strike slip component of fault motion.

The boundary conditions correspond to GPS velocity observations [3,18] (see Figs. 1 and 3). To simulate rigid plate boundaries of the area we use a rotation pole for the southern boundary corresponding to the motion of Arabia relative to Eurasia given by Vernant et al. [18]. In the Makran we do not directly model the subduction but use the velocity of the south-eastern Iranian margin relative to Eurasia to account for the differential motion between the Zagros collision and the Makran subduction. To the east and north, velocities are set to 0 to represent the lack of motion of stable Eurasia. Therefore, all results are expressed in a Eurasia reference frame. To the west, the velocities correspond to a linear evolution between the GPS sites. Horizontal velocities V_x, V_y are applied on all the vertical boundary faces, while the vertical velocity V_z is free. A mesh of 188,500 elements is used, which corresponds to an element size of 40 km.

2.3. Thermal model

Only few heat flow data are available in Iran [41]. According to a general relation between surface heat flow and tectonothermal age on the continents [42], we assume a low heat flow (i.e., ~40 mW/m^2) for stable areas (Lut, Caspian, Central Iran, Helmand, Arabia and Eurasia) and higher values of 65–70 mW/m^2 for recent mountain belts. To compute the temperature distribution with depth we use a heat production of 1.5 $\mu W/m^3$ for the upper crust, 0.5 $\mu W/m^3$ for the lower crust and 0 $\mu W/m^3$ for the mantle and assume purely conductive heat transfer. The heat flow at the base of the model is set to 10 mW/m^2, which corresponds to a shield type Moho heat flow [43,44]. We also account for the thermal effect of subduction of the Arabian mantle by computing a steady state thermal model taking into account the downwelling cold Arabian mantle lithosphere under the Zagros and the Makran (see details in Vernant and Chéry [45]). Moho temperatures are ~550 °C in the Alborz, Kopet Dag and Caucasus, ~470 °C for the Zagros, ~350 °C for the blocks and plate margins. We add some regions with steep thermal gradients to the east and north of the South Caspian block to permit localized shortening accounting for subduction of the South Caspian block, as suggested by Jackson et al. [46]. Coupled with temperature dependent rheology, our thermal model leads to brittle–ductile transitions at about ~300–350 °C [47–49] in qualitative agreement with the maximum depth of the micro-seismicity of the Zagros and Alborz mountain belts (~17–20 km) [50–52].

3. Numerical experiments

Results are presented for steady state of conditions (i.e., velocities field converges towards a final value). As we included the topography and its isostatic compensation,

Table 1
rms of the residuals velocities and fault slip rates in function of the fault friction

Experiment	Fault friction in the crust	Fault friction in the mantle	Velocity field rms (mm/yr)	Fault slip rate rms (mm/yr)
Case #1	0.02	0.02	2.5	3.3
Case #2	0.05	0.05	2.6	3.8
Case #3	0.10	0.10	2.7	4.9
Case #4	0.30	0.30	3.2	5.4
Case #5	0.02	0.30	3.0	4.5

gravitational potential energy (GPE) is created. GPE can be related to stress gradients in the lithosphere [31]. To check how GPE affects our results we have run a model with the boundary conditions set to 0 mm/yr. The results suggest that in the first stage of this model, small motions (less than 1 mm/yr) are induced by GPE suggesting that their effects are insignificant on the velocity field of our experiments. As shown by Provost et al. [6], GPE increases the normal stress on the fault plane; therefore decreasing slightly the fault slip rate. However they have shown that these changes are small, so we did not study any further the effects of GPE.

In all the following numerical experiments the effective fault friction is the only parameter which varies. We present five experiments; for four of them the effective fault friction is the same in the mantle and the crust (case #1: $\mu=0.02$, case #2: $\mu=0.05$, case #3: $\mu=0.10$, case #4: $\mu=0.30$). The fifth experiment has a low effective fault friction ($\mu=0.02$) for the crustal part of the fault and high friction ($\mu=0.30$) for the fault in the mantle (case #5).

The root mean square (rms) of the residual velocities (GPS observed − modeled velocities) and residual fault slip rates (geological − modeled slip rates) are indicated in Table 1. Strictly speaking, GPS and modeled velocities are not directly comparable. Indeed, GPS measurements in Iran are made during an interseismic period when faults are locked. However, it is usually assumed that the shape of interseismic motions around continental faults is controlled by a locking depth of about 15 km (i.e., [7,53,54]). In this case, the interseismic motion at some distance from the fault (i.e., more than 50 km) is close to the geological slip rate. Because the positions of the sites are often that far from the fault we directly compare the long-term model velocity to the observed interseismic GPS velocities. Similar rms values for the residual velocities indicate that none of the five cases presented here can be said to be the statistically optimal solution. This is due to a sparse GPS coverage, the mean distance between sites being of ~200–300 km. As a consequence, the variation of fault slip rate resulting from the change in fault friction only weakly affects the GPS site velocities. Therefore, we cannot use the differences between the GPS and the model velocities to determine a best case.

Although fault friction variation does not result in significant velocity changes at the GPS sites, it affects the fault slip rate distribution throughout the model. Therefore, we use the geologically estimated fault slip rates [55–58] as a control parameter to determine the best model. The modeled fault slip rates show large variations among the five experiments (Fig. 4 and Table 1). Case #1 ($\mu=0.02$) gives the highest slip rates on the main Iranian strike–slip faults. On the contrary, the case #4 ($\mu=0.3$) leads all the faults to be locked (i.e., their long term slip rate is 0). Cases #2 and #3, with intermediate effective fault friction, show intermediate faults slip rates. The comparison between numerical experiments and the geological estimates of the fault slip rates suggest that case #1 is the optimal model. In this experiment, the effective fault friction is so low that, for the regions with a cold geotherm (mainly the blocks), frictional fault slip occurs in the lower crust and the upper mantle (case b of the Fig. 2). Therefore, we use the case #5 to check if we can obtain fault slip rates in agreement with the geological estimations without having a discontinuity of the velocity field in the mantle under the crustal faults. To do so, we apply an effective fault friction $\mu=0.02$ in

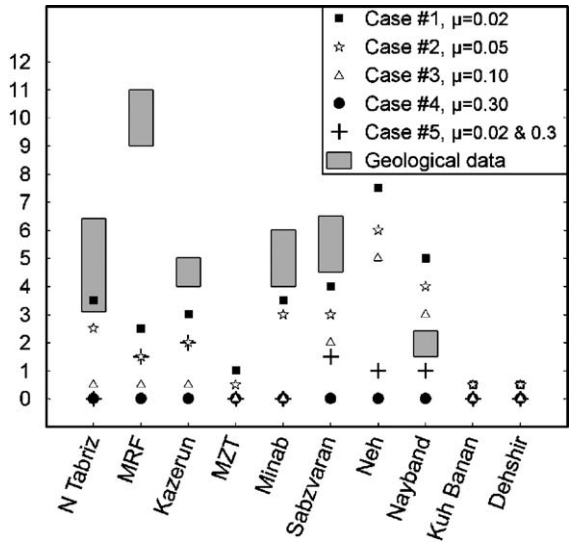

Fig. 4. Fault slip rates for the Iranian faults included in the model. The grey rectangles represent the geological estimations with their error bars. Rates obtain for the five experiments with variations of the fault friction are shown by the symbols in the inset box, upper right. Fault slip rates from Talebian and Jackson [57], Walker and Jackson [58], Hessami et al. [56], Regard (2003), and Bachmanov et al. [55].

the crust and $\mu = 0.3$ for the extent of the fault down to the mantle. The results of case #5 show much lower velocities than case #1 ($\mu = 0.02$ on the whole fault plane), and are not in agreement with geological estimates (Fig. 4).

4. Discussion

4.1. Description of the Iranian deformation

GPS coverage in Iran as shown by Vernant et al. [18] is too sparse to determine if the deformation can be described as continuum or microplate deformation. Consequently, there is a need to combine the GPS velocity field and the geological fault slip rates [55–58] to define an appropriate model of the tectonic deformation of Iran. Combining long-term observations (geological) with the short-term GPS measurement may seem inappropriate. However, we use GPS measurements on rigid plates (Arabia, Eurasia and Central Iranian Block) and far enough from the most active faults. Therefore, the GPS interseismic velocity field is only weakly influenced by the seismic cycle and so should resemble to the long-term geological velocity. We assume for the purpose of discussion that all these observations are consistent, in the same way that most of the GPS plate motions are consistent with the NUVEL-1A model [59].

The most appropriate model to describe the tectonic deformation in Iran is the numerical experiment #1, since it provides the best agreement with the geological fault slip rates (Fig. 4 and Table 1). The strain rate map and the velocity field obtained for this experiment #1 show quasi-rigid blocks (i.e., low strain rate areas) in the South Caspian (SCB), the Central Iran (CIB) and the Lut region. Low strain rates of SCB and CIB also persist in experiment #4 where all the faults are locked (i.e., continuum deformation), but they correspond to narrower quasi-rigid zones. This shrinkage of the area of the quasi-rigid block is due to the broadness of the shear zones which correspond to a diffuse deformation away from the strike–slip faults bordering the blocks. The clearest example of this is the Lut region, which becomes a large shear zone in experiment #4 (Fig. 5). Unfortunately no GPS measurements are available for this region, but instrumental and historical seismicity suggest quasi-rigid behavior of this area (Jackson and McKenzie [60]). As proposed by previous modeling experiments of the active deformation in Iran [21,22], we find quasi-rigid blocks necessary to split the deformation between southern Iran (Zagros, Makran) and the northern mountain belt (Alborz, Kopet Dag). However the direction of the velocity vectors does not seem strongly related to the block shape. Rather, geometry and velocity

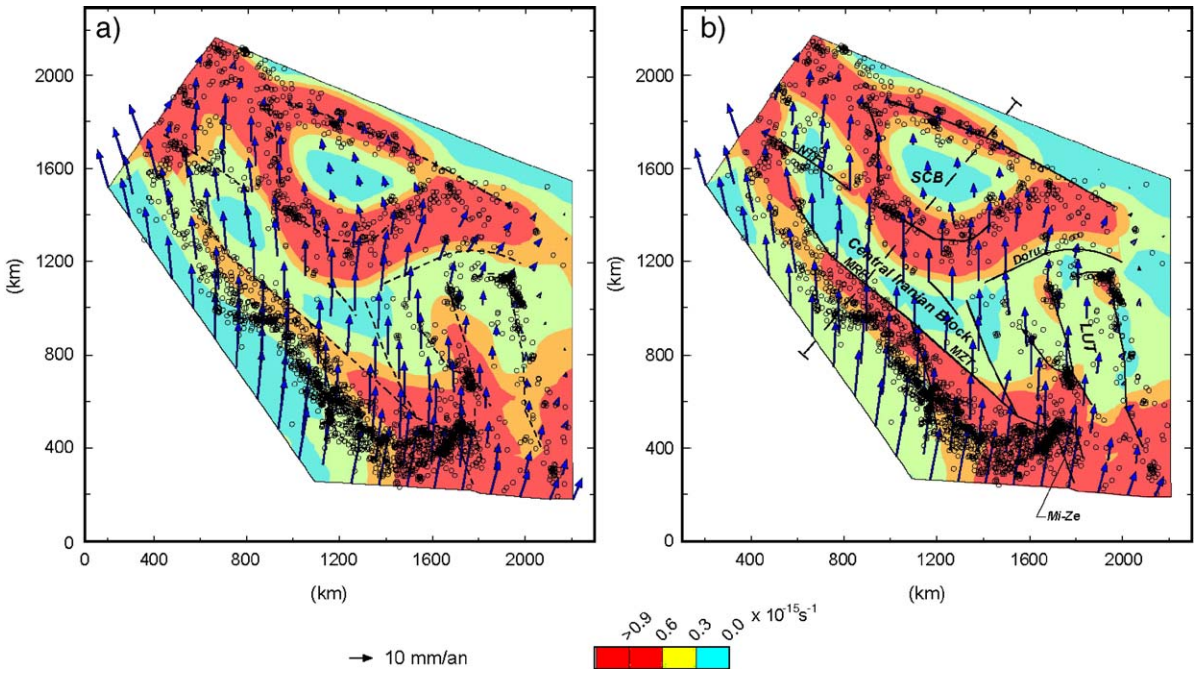

Fig. 5. Strain map and velocity field deduced from the model for two tests: (a) fault friction of 0.30; no slip occurs on the faults (case #4) and (b) fault friction of 0.02 (case #1). Strain is expressed as the square root of the second invariant of the strain rate tensor. The location of the profile of Fig. 6 is given in panel (b) by the dotted line.

of the northeastern Arabian plate boundary is more likely to determine the velocity field in Iran. This suggests that the internal kinematics of the collision is strongly controlled by the push of Arabia.

The high strain rate zones are well correlated with the seismicity. They also correspond to mountain ranges (Zagros, Caucasus, Alborz and Kopet Dag) and subduction zones (Apsheron Balkan Sills and Makran). Once again, experiment #1 displays a good agreement between strain rate and seismicity, especially for the faults surrounding the Lut block, where high strain areas near the ends of the faults are correlated with earthquake swarms (Fig. 5).

A main weakness of our modeling is the lack of dipping faults to accommodate shortening. As a result, our model cannot lead to a complete microplate description because the shortening is taken up by the continuum medium. However, if dipping faults could be added to our model, our conclusions would remain the same. Indeed, in the case #1, the deformation could be fully accommodated by a strike–slip fault, but some is still taken up by the continuum medium. This is the case for example of the Main Recent Fault (MRF) which accommodates only a part (~60%) of the Zagros range parallel component (Fig. 6). These results are in good agreement with detailed modeling of the Zagros range [45]. Moreover deformation in Iran is known to be partly aseismic [60,61], the best example being the Zagros where less than 5% of the whole deformation seems to be seismic. The structures and mechanisms accommodating the internal deformation remain unclear, but they are certainly correlated with the fact that most of the upper crust in the Zagros consists of limestone. Therefore twinning and promoting crystal–plastic mechanisms are more likely to occur at low temperature [62], creating internal deformation rather than slip on the faults. It seems that based on our results, the appropriate description of intracontinental deformation in Iran seems to be a compromise of high strain localization on faults, quasi-rigid blocks and continuum deformation within orogens. This description of the deformation agrees with the previous work of Zoback et al. [63].

4.2. Fault friction and vertical slip distribution on the fault plane

Our best model (experiment #1) implies very low fault friction on the main Iranian strike slip faults. The corresponding effective friction is $\mu = 0.02$, consistent with the low values suggested for other strike–slip faults such as the North Anatolian fault [6] or the San Andreas fault (e.g., [64–67]). However, the Nayband fault (Fig. 4) could have a higher fault friction since the slip rate obtained with $\mu = 0.02$ is too high. On the other hand, we could not fit the high slip rate of the Main Recent Fault (Fig. 4). This could be due to an underestimation of the time span guessed by the authors to estimate the fault slip rate, indeed neither Talebian and Jackson [57], nor Bachmanov et al. [55] have geochronological dating constraints in their studies.

In experiment #5 in which the effective fault friction is high for the upper mantle part of the fault (0.3) and low in the crust (0.02), fault slip rates seem generally to be lower than geological estimates. Therefore, a low fault friction is also needed in the mantle. This may imply that slip may occur in the mantle or that a localized strain zone develops in response to a low strength of the fault zone (Fig. 2). Experiment #1 suggests two types of faults: (1) fault

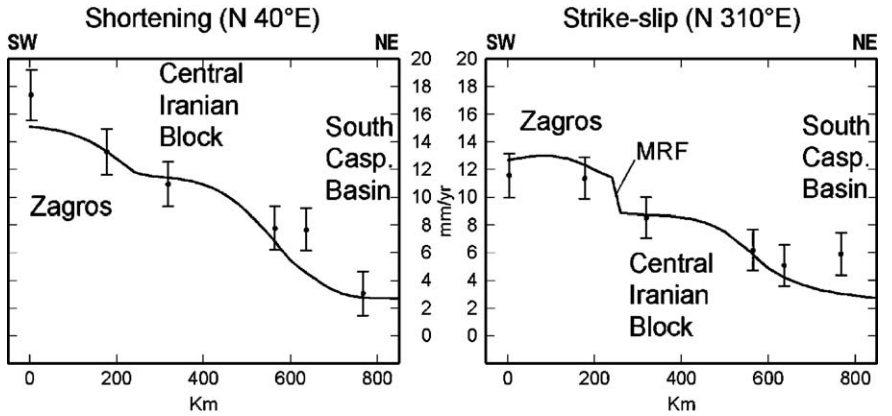

Fig. 6. Velocity profiles across the Zagros, the Main Recent Fault (MRF), the Central Iranian Block and the South Caspian basin, (a) Zagros range perpendicular profile (shortening), (b) range parallel profile (strike–slip). The GPS velocities are given with their 1σ uncertainties (Vernant et al. [18]).

planes where slip occurs in the upper mantle and (2) faults where the slip is limited to the upper crust. These two types are dependent on the geotherm of the region. In a mountain range, a high temperature gradient allows decoupling of upper crust and upper mantle (i.e., that the mantle does not exert a strong shear traction on the crust since there is a layer of low viscosity between the mantle and the upper crust, as opposed to delamination which means that the mantle is kinematically and physically detached from the crust), confining slip in the upper crust only. Along faults bordering quasi-rigid blocks, the geotherms usually are like those of continental shields. No decoupling should occur and fault slip extents down into the upper mantle. In that way our model is probably not realistic, but this experiment may suggest that the deformation below crustal faults needs to be concentrated in narrow shear zones in the mantle when the geotherm is cold. Several hypotheses can be discussed to support such an interpretation. First, Iranian mantle shear zones are often correlated with old oceanic sutures [68]. Therefore, remnant serpentines could be underneath the crustal faults acting as weak zones for the strike slip motion, as it has been suggested from the exhumation of subducted rocks in Himalaya [69]. Second, shear heating is more likely to occur when the geotherm is low for the intracontinental strike–slip zones [70] leading to a well localized shear zone between the upper mantle parts of continental blocks. A non-linear strain rate–stress relation for mantle rocks suggested by laboratory experiments [71] could also help localize deformation under crustal faults.

4.3. Driving forces of the Arabia/Eurasia collision

Our model does not allow us to address the problem of the driving forces causing tectonic deformation and uplift of the Iranian mountain ranges. Nevertheless, setting-up boundary conditions for the motion of Arabia relative to Eurasia is equivalent to inducing a push coming from Arabian plate motion. We do not discuss here if this push is due to a remnant Neotethys slab under the Zagros pulling Arabia, or a ridge push due to opening of the Red Sea. Rather, we debate if the push of Arabia can explain the kinematics of intracontinental deformation of Iran. Our model results are in good agreement with the GPS velocity almost everywhere except in the Caucasus, North West Iran and the South Caspian region. Although we included an easily deformable area west of the South Caspian region in order to simulate the shortening due to likely subduction of the South Caspian block under the Kura basin [46,72], we cannot explain the eastward component of the sites in the Kura basin. Moreover, we are not able to obtain a westward motion of the South Caspian Block, as suggested by the kinematic reconstruction of Jackson et al. [46]. Therefore, it seems that the push of Arabia can explain most of kinematics features of Iran (Zagros, Makran, Lut, Kopet Dag), but it fails to reproduce the complex velocity field in Caucasus and South Caspian regions.

Pull of a remnant slab of an ancient subduction under the western Caucasus (e.g., [73]) could provide an explanation for the velocity field in the Kura basin. Moreover, it seems clear that as suggested by Jackson et al. [46], a western motion of the South Caspian Block relative to central Iran or Eurasia is needed to explain left lateral motion in the central Alborz range as suggested by Allen et al. [72,74] and Ritz et al. [75]. Two possibilities could explain the westward motion of the SCB: (1) the South Caspian Block is squeezed between the Alborz and the Kopet Dag and ejected to the west; (2) a remnant part of the oceanic crust under the Talesh and the Kura basin is pulling the block to the west.

5. Conclusions

These modeling experiments suggest that available GPS data in Iran are too sparse to determine precisely the style of deformation which occurs in Iran. However, it seems that neither microplate nor continuum description can fully explain the observed velocity field. We suggest that deformation in Iran is a mix between microplate and continuum deformation, combining quasi-rigid blocks, diffuse deformation zone in orogens and motion on large strike–slip faults. Due to the still sparse GPS coverage, we cannot infer precisely the deformation of the Iranian mountain ranges.

Combining the GPS velocity field with the geological fault slip rate estimates leads to a very low fault friction ($\mu = 0.02$) in order to fit slip rate values. This finding is in good agreement with the low fault friction proposed for some other intracontinental strike–slip faults (e.g., [6,64–67,76]). We suggest that localized shear zones occur in the mantle underneath crustal strike–slip fault zones for the region with a low geotherm (at borders of quasi-rigid blocks). This type of fault may be correlated with old oceanic sutures where presence of serpentine [69] as well as shear heating [70] could significantly weaken ductile shear in the upper mantle.

The northward directed push of Arabia towards Eurasia explains most of the kinematics Iran, except for the Kura and South Caspian basins where other forces seem to influence the surface velocity field. We conjecture that some remnant parts of old oceanic lithosphere under the Caucasus and the Kura basin can create slab pull in these regions.

Acknowledgements

We thank W. Thatcher, N. Fay and an anonymous reviewer for their helpful reviews. This work was supported by the "Intérieur de la Terre" INSU-CNRS program.

References

[1] W. Thatcher, Microplate versus continuum descriptions of active tectonic deformation, J. Geophys. Res. 100 (1995) 3885–3894.
[2] F. Flerit, et al., Slip partitioning in the Sea of Marmara pull-apart determined from GPS velocity vectors, J. Geophys. Res. 154 (1) (2003) 1–7.
[3] S. McClusky, et al., GPS constraints on plate motions and deformations in eastern Mediterranean and Caucasus, J. Geophys. Res. 105 (2000) 5695–5719.
[4] B.J. Meade, et al., Estimates of seismic potential in the Marmara Sea regions from block models of secular deformation constrained by global positioning system measurements, Bull. Seismol. Soc. Am. 92 (1) (2002) 208–215.
[5] M. Nyst, W. Thatcher, New constraints on the active tectonic deformation of the Aegean, J. Geophys. Res. 109 (B11) (2004) 23.
[6] A.-S. Provost, J. Chéry, R. Hassani, 3D mechanical modelling of the GPS velocity field along the North Anatolian fault, Earth Planet. Sci. Lett. 209 (2003) 361–377.
[7] R. Reilinger et al., GPS Constraints on Continental Deformation in the Africa–Arabia–Eurasia Continental Collision Zone and Implications for the Dynamics of Plate Interactions. J. Geophys. Res. (in press).
[8] S.M. McClusky, et al., Present day kinematics of the Eastern California shear zone form a geodetically constrained block model, Geophys. Res. Lett. 28 (17) (2001) 3369–3372.
[9] J.-P. Avouac, P. Tapponnier, Kinematic model of active deformation in central Asia, Geophys. Res. Lett. 20 (1993) 895–898.
[10] G. Peltzer, F. Saucier, Present-day kinematics of Asia derived from geologic fault rates, J. Geophys. Res. 101 (B12) (1996) 27943–27956.
[11] P. Tapponnier, et al., Propagating extrusion tectonics in Asia: new insights from simple experiments with plasticine, Geology 10 (1982) 611–616.
[12] P.C. England, G.A. Houseman, Finite strain calculations of continental deformation: 2. Comparison with the India–Asia collision zone, J. Geophys. Res. 91 (1986) 3664–3676.
[13] P.C. England, P. Molnar, Active deformation of Asia: from kinematics to dynamics, Science 278 (1997) 647–650.
[14] Q. Wang, et al., Present-day crustal deformation in China by global positioning system measurements, Science 294 (2001) 574–577.
[15] F. Nilforoushan, et al., GPS networks monitors the Arabia–Eurasia collision deformation in Iran, J. Geod. 77 (2003) 411–422.
[16] M. Tatar, et al., The present-day deformation of the central Zagros from GPS measurements, Geophys. Res. Lett. 29 (19) (2002) 1927, doi:10.1029/2002GL015427.
[17] P. Vernant, et al., Deciphering oblique shortening of central Alborz in Iran using geodetic data, Earth Planet. Sci. Lett. 223 (1–2) (2004) 177–185.
[18] P. Vernant, et al., Contemporary Crustal Deformation and Plate Kinematics in Middle East Constrained by GPS measurements in Iran and Northern Oman, Geophys. J. Int. 157 (2004) 381–398.
[19] N. McQuarrie, et al., Cenozoic evolution of Neotethys and implications for the causes of plate motions, Geophys. Res. Lett. 30 (20) (2003), doi:10.1029/2003GL017992.
[20] M. Allen, J. Jackson, R. Walker, Late Cenozoic reorganization of the Arabia–Eurasia collision and the comparison of short-term and long-term deformation rates, Tectonics 23 (2) (2004) 16.
[21] J.A. Jackson, J. Haines, W. Holt, The accommodation of the Arabia–Eurasia plate convergence in Iran, J. Geophys. Res. 100 (1995) 15205–15219.
[22] F. Sobouti, J. Arkani-Hamed, Numerical modelling of the deformation of the Iranian plateau, Geophys. J. Int. 126 (1996) 805–818.
[23] C. Beaumont, G. Quinlan, A geodynamic framework for interpreting crustal-scale seismic-reflectivity patterns in compressional orogens, Geophys. J. Int. 116 (1994) 754–783.
[24] P. Bird, Finite element modeling of the lithosphere deformation: the Zagros collision orogeny, Tectonophysics 50 (1978) 307–336.
[25] P. Bird, Testing hypotheses on plate-driving mechanisms with global lithosphere models including topography, thermal structure, and faults, J. Geophys. Res. 103 (B5) (1998) 10115–10130.
[26] P. Bird, J. Baumgardner, Fault friction, regional stress, and crust–mantle coupling in southern California from finite element methods, J. Geophys. Res. 89 (1984) 1932–1944.
[27] R. Hassani, D. Jongmans, J. Chéry, Study of plate deformation and stresses in subduction processes using two-dimensional numerical models, J. Geophys. Res. 102 (1997) 17951–17965.
[28] J. Braun, Three-dimensional numerical simulations of crustal-scale wrenching using a non-linear failure criterion, J. Struct. Geol. 16 (8) (1994) 1173–1186.
[29] J. Chéry, M.D. Zoback, R. Hassani, An integrated mechanical model of the San Andreas Fault in central and northern California, J. Geophys. Res. 106 (2001) 22051–22066.
[30] J.C. Lynch, M.A. Richards, Finite element models of stress orientations in well-developed strike–slip fault zones: implications for the distribution of lower crustal strain, J. Geophys. Res. 106 (2001) 26707–26729.
[31] P.C. England, D.P. McKenzie, A thin viscous sheet model for continental deformation, Geophys. J. R. Astron. Soc. 73 (1982) 523–532.
[32] J. Chéry, H. Hassani, ADELI: a 2D/3D Finite Element Software for the Thermomechanical Modeling of the Geological Deformation, 2002, p. 25.
[33] Y. Leroy, M. Ortiz, Finite element analysis of strain localization in frictional materials, Int. J. Numer. Anal. Methods Geomech. 13 (1989) 53–74.
[34] N.L. Carter, M.C. Tsenn, Flow properties of continental lithosphere, Tectonophysics 136 (1987) 27–63.
[35] S.H. Kirby, A.K. Kronenberg, Rheology of the lithosphere: selected topics, Rev. Geophys. 25 (6) (1987) 1219–1244.
[36] M.C. Tsenn, N.L. Carter, Upper limits of power law creep of rocks, Tectonophysics 136 (1987) 1–26.
[37] J. Strehlau, R. Meissner, Estimation of crustal viscosities and shear stresses from an extrapolation of experimental steady state flow data, in: K. Fuchs, C. Froidevaux (Eds.), Composition, Structure, and Dynamics of the Lithosphere–Asthenosphere System, AGU, Washington, D.C., 1987, pp. 66–87.
[38] P. Bird, X. Kong, Computer simulations of California tectonics confirm very low strength of major faults, Geol. Soc. Amer. Bull. 106 (2) (1994) 159–174.
[39] P.A. Cundall, M. Board, A microcomputer program for modelling large-strain plasticity problems, International Conference on Numerical Methods in Geomechanics, 1988.
[40] G.A. Dehghani, J. Makris, The gravity field and crustal structure of Iran, N. Jahrb. Geol. Palaont. Abh. Stuttgart 168 (1984) 215–229.

[41] H.N. Pollack, S.J. Hurter, J.R. Johnson, Heat flow from the Earth's interior; analysis of the global data set, Rev. Geophys. 31 (3) (1993) 267–280.
[42] P. Morgan, J.H. Sass, Thermal regime of the continental lithosphere, J. Geodyn. 1 (1984) 143–166.
[43] C. Pinet, C. Jaupart, The vertical distribution of radiogenic heat production in the Precambrian crust of Norway and Sweden: geothermal implications, Geophys. Res. Lett. 14 (1987) 260–263.
[44] C. Pinet, et al., Heat flow and structure of the lithosphere in the Eastern Canadian shield, J. Geophys. Res. 96 (1991) 19941–19963.
[45] P. Vernant, J. Chéry, Mechanical modelling of oblique convergence in the Zagros, Iran. Geophys. J. Int. (in press).
[46] J.A. Jackson, et al., Active tectonics of the South Caspian Basin, Geophys. J. Int. 148 (2002) 214–245.
[47] W.P. Chen, P. Molnar, Focal depths of the intracontinental and intraplate earthquakes and their implications for the thermal and mechanical properties of the lithosphere, J. Geophys. Res. 88 (1983) 4183–4214.
[48] R. Meissner, J. Strehlau, Limits of stresses in continental crusts and their relation to depth–frequency distribution of shallow earthquakes, Tectonics 1 (1) (1982) 73–89.
[49] R.H. Sibson, Fault zone models, heat flow, and the depth distribution of earthquakes in the continental crust of the United States, Bull. Seismol. Soc. Am. 72 (1) (1983) 151–163.
[50] M. Ashtari, D. Hatzfeld, N. Kamalian, Microseismicity in the region of Tehran, Tectonophysics 395 (3–4) (2005) 193–208.
[51] A. Maggi, et al., A re-assessment of focal depth distribution in southern Iran, the Tien Shan and northern India: do earthquakes really occur in the continental mantle? Geophys. J. Int. 143 (2000) 629–661.
[52] M. Tatar, D. Hatzfeld, M. Ghafori-Ashtiany, Tectonics of the Central Zagros (Iran) deduced from microearthquake seismicity, J. Geophys. Res. 156 (2) (2004) 255–266.
[53] J. Savage, R. Burford, Geodetic determination of relative plate motion in Central California, J. Geophys. Res. 95 (1973) 4873–4879.
[54] T. Wright, B. Parsons, E. Fielding, Measurement of interseismic strain accumulation across the North Anatolian Fault by satellite radar interferometry, Geophys. Res. Lett. 28 (10) (2001) 2117–2120.
[55] D.M. Bachmanov, et al., Active faults in the Zagros and central Iran, Tectonophysics 380 (3–4) (2004) 221–241.
[56] K. Hessami, et al., Paleoearthquakes and slip rates of the Northern Tabriz fault, NW Iran: preliminary results, Ann. Geophys. 46 (5) (2003) 903–915.
[57] M. Talebian, J.A. Jackson, Offset on the Main Recent Fault of the NW Iran and implications for the late Cenozoic tectonics of the Arabia–Eurasia collision zone, Geophys. J. Int. 150 (2002) 422–439.
[58] R. Walker, J.A. Jackson, Offset and evolution of the Gowk fault, S.E. Iran: a major intra-continental strike–slip system, J. Struct. Geol. 24 (2002) 1677–1698.
[59] G.F. Sella, T.H. Dixon, A. Mao, REVEL: a model for recent plate velocities from space geodesy, J. Geophys. Res. 107 (B4) (2002) ETG 11-1–ETG 11-32.
[60] J.A. Jackson, D.P. McKenzie, The relationship between plate motions and seismic tensors, and the rates of active deformation in the Mediterranean and Middle East, Geophys. J. R. Astron. Soc. 93 (1988) 45–73.
[61] F. Masson, et al., Seismic versus aseismic deformation in Iran inferred from earthquakes and geodetic data, Geophys. J. Int. 160 (1) (2005) 217–226.
[62] L.A. Kennedy, J.C. White, Low-temperature recrystallization in calcite; mechanisms and consequences, Geology (Boulder) 29 (11) (2001) 1027–1030.
[63] M.D. Zoback, J. Townend, B. Grollimund, Steady-state failure equilibrium and deformation of intraplate lithosphere, Int. Geol. Rev. 44 (5) (2002) 383–401.
[64] A.-S. Provost, H. Houston, Orientation of the stress field surrounding the creeping section of the San Andreas fault: evidence for a narrow mechanically-weak fault zone, J. Geophys. Res. 106 (2001) 11373–11386.
[65] J. Townend, M.D. Zoback, Implications of earthquake focal mechanisms for the frictional strength of the San Andreas fault system, Geological Society Special Publications, vol. 186, 2001, pp. 13–21.
[66] J. Townend, M.D. Zoback, Regional tectonic stress near the San Andreas fault in central and southern California, Geophys. Res. Lett. 31 (2004), doi:10.1029/2003GL018918.
[67] M.D. Zoback, et al., New evidence on the state of stress of the San Andreas fault system, Science 238 (1987) 1105–1111.
[68] G.K. Lensch, K. Schmidt, M. Davoudzadeh, Introduction to the geology of Iran, N. Jahrb. Geol. Palaont. Abh. Stuttgart 168 (1984) 155–164.
[69] S. Guillot, K.H. Hattori, J. Sigoyer, Mantle wedge serpentinization and exhumation of eclogites: insights from eastern Ladakh, northwest Himalaya, Geology 28 (3) (2000) 199–202.
[70] P.H. Leloup, et al., Shear heating in continental strike–slip shear zones: model and field examples, Geophys. J. Int. 136 (1999) 19–40.
[71] D.L. Kohlstedt, B. Evans, S.J. Mackwell, Strength of the lithosphere: constraints imposed by laboratory experiments, J. Geophys. Res. 100 (B9) (1995) 17587–17602.
[72] M.B. Allen, et al., Late Cenozoic deformation in the South Caspian region: effects of a rigid basement block within a collision zone, Tectonophysics 366 (2003) 223–239.
[73] J. Dercourt, et al., Geological evolution of the Tethys belt from the Atlantic to the Pamirs since the Lias, Tectonophysics 123 (1986) 241–315.
[74] M. Allen, et al., Accommodation of late Cenozoic oblique shortening in the Alborz range, Iran, J. Struct. Geol. 25 (2003) 659–672.
[75] J.-F. Ritz, et al., Active transtension inside Central Alborz: a new insight into the Northern Iran–Southern Caspian geodynamics. Geology (in press).
[76] V.S. Mount, J. Suppe, State of stress near the San Andreas fault: implications for the wrench tectonics, Geology 15 (1987) 1143–1146.